Assessment of metrics that measure the effectiveness of control allocation and their use in linear closed-loop analysis

Umut Zalluhoglu*, Raghu Venkataraman, Marco Ceze, Hugh Carson, Michael Szmuk, Christopher McFarland, and David Friedman
Amazon, Seattle, WA

This paper assesses several metrics that measure the effectiveness of control allocation algorithms. These algorithms are used in aerospace systems where virtual control inputs need to be allocated among multiple actuators, e.g., the allocation of rolling moment among multiple ailerons on an aircraft wing. The only assumptions made on the control allocation algorithm are that (1) it is continuously differentiable throughout its domain and (2) it is scheduled using a measurement of the operating condition of the system. Each proposed metric is expressed as some measure of a matrix that is computed from the respective linearizations of the plant and the control allocation algorithm. The paper makes four contributions. First, it shows how some of the proposed metrics are correlated with the performance and robustness metrics that are computed during linear closed-loop analysis. Second, it presents how the proposed metrics are correlated with the grid density of the scheduling variables used in the control allocation algorithm. Third, it shows how some of the proposed metrics can be used to detect sign reversals in the control effectiveness of individual actuators. Fourth, it shows how the metrics may be adjusted to account for failures in one or more actuators. These contributions are demonstrated using a fixed-wing aircraft model. While the focus of the paper is in applying these metrics for analysis, the metrics may also be used to aid the design of the control allocation algorithm.

I. Introduction

Modern aerospace systems often feature multiple actuators, some of which may be redundant, to meet extremely demanding requirements on reliability and maneuverability. For example, the Boeing 777 has 14 spoilers each with its own actuator; two actuators each for the outboard ailerons, elevators, and flaperons; and three actuators for the single rudder [1]. The system is said to be over-actuated if the number of available actuators exceeds the degrees of freedom to be controlled, i.e., if there are multiple ways to allocate the actuators to achieve the same state in the control degrees of freedom. The desired state in the control degrees of freedom may be interpreted as a virtual control command. Control allocation algorithms are used in such scenarios to optimally allocate the available actuators to achieve the virtual control commands corresponding to the desired state in the control degrees of freedom. This requires the control allocator, together with flight control law, to be implemented in the overall flight control system.

Conventional flight control laws are designed to generate one virtual control command for each controlled degree of freedom. The control allocator is responsible for distributing these commands among multiple redundant actuators. In addition to achieving the requested commands from the controller, control allocators for over-actuated systems are designed to meet additional goals such as drag minimization, gust load alleviation, and minimizing power consumption, while being subject to constraints on the actuator position and rate limits [2, 3]. The flight control law and/or the control allocator may also be scheduled using one or more measurements of the operating condition to account for model variations over the operating envelope of the system [4, 5].

The control allocation problem has been intensively studied in the literature and various allocation techniques have been developed over the past three decades. Unconstrained linear control allocation methods such as pseudo-inverse are introduced in [6], followed by constrained linear control allocation methods such as daisy chaining [7] and direct control allocation [8]. More complex and customizable structures like linear and quadratic programming are leveraged in [9] and [10]. Nonlinear programming methods are proposed in [11], [12] and [13]. A comprehensive survey on the control allocation methods can be found in [14].

In the event of one or more actuator failures, the virtual control commands need to be effectively re-allocated among the remaining healthy actuators in order to maintain acceptable performance [15]. If this re-allocation is properly

*Research Scientist, Amazon.

achieved, then the actuator failures may be compensated without reconfiguring the flight control law. In other words, if the physical aircraft changes due to a failure, then the control allocation algorithm can potentially abstract this change from the controller [16]. In this regard, it is common practice to separately design the flight control law and control allocation algorithm as components of the overall flight control system [17]. This decomposition allows one to analyze the performance of the control allocator in isolation.

In this context, this paper proposes several metrics to measure the effectiveness of control allocation algorithms that are continuously differentiable throughout the operating envelope and are scheduled using a measurement of the operating condition of the system. For simplicity, the flight control law is intentionally not scheduled using the measurement of the operating condition of the system. This helps keep the focus of the paper on assessing the effectiveness of the control allocation algorithm as the control derivatives vary across the operating envelope. As its main contributions, the paper shows how these proposed metrics:

1) are correlated with the key linear closed-loop performance and robustness metrics,
2) are correlated with the grid density of the scheduling variables used in the control allocation algorithm,
3) can be used to detect sign reversals in the control effectiveness of individual actuators, and
4) can be adjusted to account for saturation or failures in one or more actuators.

In addition to providing a tool to assess the effectiveness of control allocation algorithms and their impact on linear closed-loop performance and robustness, the proposed metrics can also guide the design of such algorithms.

This paper is organized as follows: Section II presents the problem statement and Section III presents the proposed metrics that measure the effectiveness of control allocation algorithms. Section IV introduces a numerical example involving the lateral-directional flight dynamic model of a small fixed-wing unmanned aircraft called the UltraStick 25e that was reported in [18]. Section V applies the proposed metrics to this numerical example and demonstrates the aforementioned contributions of the paper. Finally, Section VI concludes the paper.

II. Problem formulation

A. General closed-loop system

Consider the block diagram representation of the general closed-loop system shown in Figure 1. There are three basic components: the plant G, the actuator dynamics Λ, and the controller K. The outputs $\boldsymbol{y} \in \mathbb{R}^{n_y}$ of the plant G are fed to the feedback controller K along with the reference commands $\boldsymbol{r} \in \mathbb{R}^{n_r}$. The feedback controller uses $\boldsymbol{r}$ and $\boldsymbol{y}$ to generate the actuator commands $\boldsymbol{u}_{cmd} \in \mathbb{R}^{n_u}$. The actuator dynamics Λ converts $\boldsymbol{u}_{cmd}$ into the true actuator inputs $\boldsymbol{u} \in \mathbb{R}^{n_u}$ to the plant G. The blocks K, Λ, and G are represented as linear, time-invariant (LTI) dynamical systems, as shown by their functional dependence on the Laplace variable s. Additionally, the linearizations of the plant and the controller are functions of the operating condition $\rho \in \mathcal{P}$. An imperfect measurement $\rho_m = m(\rho)$, $m : \mathcal{P} \to \mathcal{P}$ of the operating condition is used to schedule the controller K across the operating envelope $\mathcal{P}$. For notational simplicity, functions (e.g., $m(\rho)$) are overloaded to also mean the value of the function evaluated at a specific input. The interpretation should be clear from the context.

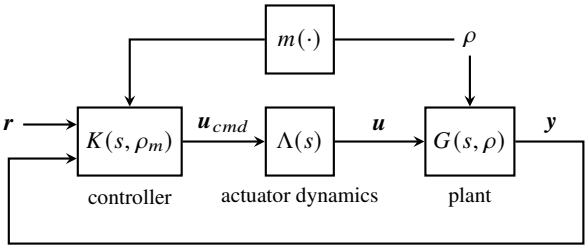

Fig. 1 General closed-loop system.

The typical control design problem involves synthesizing $K(s, \cdot)$ to satisfy several user-defined closed-loop performance and robustness requirements across a discrete set of N plant models $\{G(s, \rho_i) \mid \rho_i \in \mathcal{P}\}_{i=1}^{N}$. This problem has been widely studied and there are several classical and modern control design techniques to directly synthesize $K(s, \cdot)$ [19]. However, the problem may be simplified by explicitly considering the control degrees of freedom $\boldsymbol{v} \in \mathbb{R}^{n_v}$, which are an abstract representation of the control input to the plant. (For example, the rolling moment command in a fixed-wing aircraft is a control degree of freedom whereas the aileron deflection is an actuator input.) The relative order

between the number of actuators n_u and the control degrees of freedom n_v dictates whether the plant is over-actuated ($n_u > n_v$), fully-actuated ($n_u = n_v$), or under-actuated ($n_u < n_v$). The control degrees of freedom enable the separation of the task of control allocation from the task of feedback control [20], as shown in Figure 2.

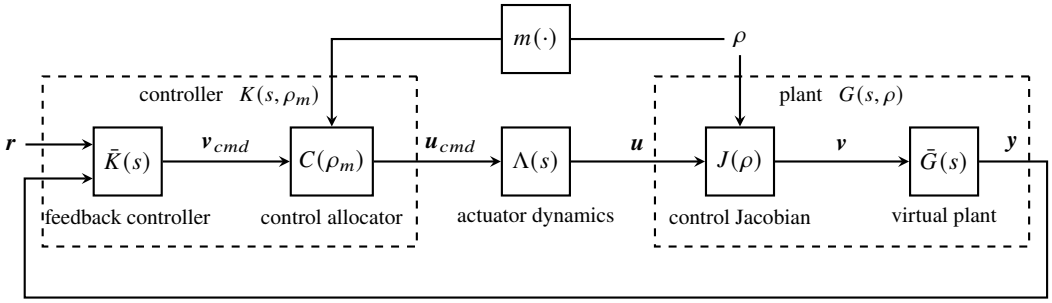

Fig. 2 Decomposition of the controller and the plant.

Specifically, the controller $K(s,\rho_m)$ is decomposed into a feedback controller $\bar{K}(s)$ that generates the virtual control commands $\boldsymbol{v}_{cmd} \in \mathbb{R}^{n_v}$ that span the control degrees of freedom and a control allocator $C(\rho_m)$ that maps them into the actuator commands $\boldsymbol{u}_{cmd}$. Similarly, the plant $G(s,\rho)$ is decomposed into a control Jacobian $J(\rho)$ that maps the true actuator inputs $\boldsymbol{u}$ into the virtual control inputs $\boldsymbol{v} \in \mathbb{R}^{n_v}$ that span the control degrees of freedom, and a virtual plant $\bar{G}(s)$ that maps $\boldsymbol{v}$ into the outputs $\boldsymbol{y}$. These decompositions, along with a few assumptions, allow for the design of the feedback controller $\bar{K}(s)$ to be decoupled from the design of the control allocator $C(\rho_m)$. These assumptions are discussed next.

B. Assumptions

Assumption 1 *Each component of the closed-loop system is assumed to be a continuously-differentiable nonlinear function of its inputs and the operating condition ρ. This is needed to be able to compute linearizations for analysis.*

Assumption 2 *The virtual plant $\bar{G}(s)$ is intentionally assumed to be independent of the operating condition ρ, and the feedback controller $\bar{K}(s)$ is not scheduled on the measurement ρ_m.*

This assumption is not necessary in order to be able to apply the metrics that will be developed in Section III to practical problems. These metrics are functions of only $C(\rho_m)$ and $J(\rho)$. However, this assumption is intentionally made to limit the scope of the paper to the study of the effectiveness of the control allocator as the control Jacobian $J(\rho)$ varies across the operating envelope $\mathcal{P}$. Specifically, this assumption helps avoid the need to also study the impact of scheduling $\bar{K}(s)$ over the operating envelope, since that is not the focus of the paper.

Given this assumption, the linearization of the plant $G(s,\rho)$ is expressed as:

$$\dot{\boldsymbol{x}} = A\boldsymbol{x} + BJ(\rho)\boldsymbol{u} \tag{1a}$$

$$\boldsymbol{y} = C\boldsymbol{x} + DJ(\rho)\boldsymbol{u} \tag{1b}$$

where $A \in \mathbb{R}^{n_x \times n_x}$, $B \in \mathbb{R}^{n_x \times n_v}$, $C \in \mathbb{R}^{n_y \times n_x}$, and $D \in \mathbb{R}^{n_y \times n_v}$ represent a state-space realization of $\bar{G}(s)$.

Assumption 3 *The control Jacobian $J(\rho)$ and the control allocator $C(\rho_m)$ are assumed to be static systems with no internal state.*

Assumption 4 *The actuator dynamics $\Lambda(s)$ is assumed to be diagonal: $\Lambda(s) = \bar{\Lambda}(s) \cdot \mathrm{diag}(\boldsymbol{h})$*, where $\bar{\Lambda}(s)$ is a single-input single-output LTI system and $\boldsymbol{h} \in \mathbb{R}^{n_u}$ is a vector of ones and zeros that stores the health of each actuator, i.e., $\boldsymbol{h}_i \in \{0,1\}$ for $i = 1,\ldots,n_u$.*

This assumption implies that all the actuation channels are independent but share the same model. This assumption is made in order to be able to decouple the design of $\bar{K}(s)$ from that of $C(\rho_m)$. If this assumption is violated, then the

*diag denotes an operator that acts on both vectors and square matrices. When operating on vectors, it returns a square matrix with the elements along the diagonal. When operating on square matrices, it returns a vector with the diagonal elements.

control allocation effectiveness metrics developed in Section III would need to be made frequency-dependent so as to include $\Lambda(s)$. As discussed in Section III.C.3, frequency-dependent metrics are not within the scope of this paper.

The vector $\boldsymbol{h}$ captures both the effects of saturations and failures in the actuators. Specifically, if the i^{th} actuator is saturated or failed, then $\boldsymbol{h}_i = 0$ captures the fact that the loop-gain is zero in that channel. Therefore, if n_{u_f} denotes the total number of saturated and failed actuators, then $\sum_{i=1}^{n_u} \boldsymbol{h}_i = n_u - n_{u_f}$ denotes the total number of actuators available for allocation.

Assumption 5 *The feedback controller $\bar{K}(s)$ is designed under the assumption that the control allocator $C(\rho_m)$ perfectly allocates the virtual control commands $\boldsymbol{v}_{cmd}$ among the actuators available for allocation. For example, if $n_u - n_{u_f} \geq n_v$, then $J(\rho) \cdot \text{diag}(\boldsymbol{h}) \cdot C(\rho_m) = I_{n_v}$.*

This assumption is made in order to be able to decouple the design of $\bar{K}(s)$ from that of $C(\rho_m)$. It is not necessary in order to conduct linear analysis of the entire closed-loop system.

C. Decoupling the design of $\bar{K}$ and C

The decompositions discussed in Section II.A and the assumptions made in Section II.B allow for a decoupled control design process wherein the feedback controller $\bar{K}(s)$ is designed only using the virtual plant $\bar{G}(s)$, and the control allocator $C(\rho_m)$ is designed only using the control Jacobian $J(\rho_m)$. This is shown in Figure 3.

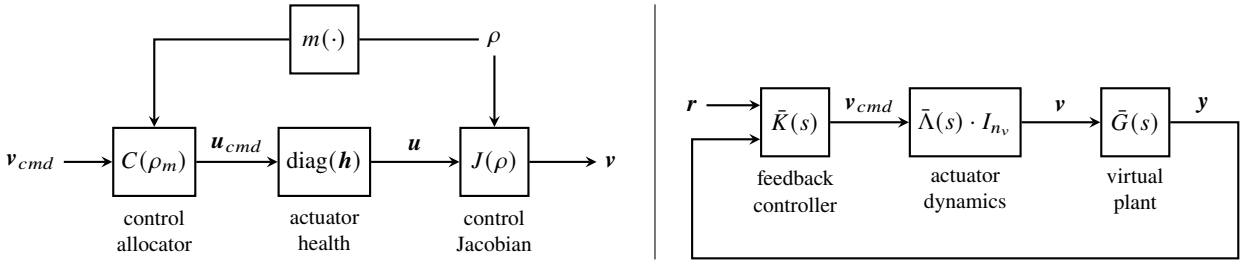

Fig. 3 Control allocator design (left) and feedback controller design (right).

Figure 3 is essentially a block diagram manipulation of Figure 2, where Assumption 4 is used to commute $\bar{\Lambda}(s)$:

$$J(\rho) \cdot \Lambda(s) \cdot C(\rho_m) \;=\; J(\rho) \cdot \left(\bar{\Lambda}(s) \cdot \text{diag}(\boldsymbol{h})\right) \cdot C(\rho_m) \;=\; J(\rho) \cdot \text{diag}(\boldsymbol{h}) \cdot C(\rho_m) \cdot \left(\bar{\Lambda}(s) \cdot I_{n_v}\right) \tag{2}$$

and Assumption 5 is used to lift the product $J(\rho) \cdot \text{diag}(\boldsymbol{h}) \cdot C(\rho_m)$ out of the feedback loop.

Therefore, given the virtual plant $\bar{G}(s)$, the feedback controller $\bar{K}(s)$ is designed using standard control design techniques to satisfy the user-defined closed-loop performance and robustness requirements. The control allocator $C(\rho_m)$ is separately designed using the control Jacobian $J(\rho)$.

Since the decoupling of the control design process relies on Assumption 5, it is important to develop metrics that quantify the effectiveness with which any given control allocator satisfies the assumption $J(\rho) \cdot \text{diag}(\boldsymbol{h}) \cdot C(\rho_m) = I_{n_v}$. Deficiencies in the control allocation will not only lead to a violation of Assumption 5, but will also impact the closed-loop performance and robustness metrics, which are ultimately what matter. Therefore, any metrics that are developed for this purpose must not only quantify the effectiveness of control allocation in terms of Assumption 5, but must also correlate strongly with the closed-loop performance and robustness metrics that are calculated using the original closed-loop system shown in Figure 1. The next section develops a few metrics for this purpose.

III. Metrics that measure the effectiveness of control allocation

A. Commanded-to-actual virtual control matrix

At a given operating condition ρ, the metrics are computed using the product $W(\rho) \coloneqq J(\rho) \cdot \text{diag}(\boldsymbol{h}) \cdot C(\rho_m) \in \mathbb{R}^{n_v \times n_v}$, where $J(\rho)$ denotes the control Jacobian, $C(\rho_m)$ denotes the linearization of the control allocator, and $\boldsymbol{h}$ is a vector of ones and zeros storing the health of each actuator. The presence of $\text{diag}(\boldsymbol{h})$ in this product implies that $\text{rank}\, W(\rho) = \min(n_u - n_{u_f}, n_v)$. The product $W(\rho)$ is termed as the *commanded-to-actual virtual control matrix* because it maps the virtual control commands $\boldsymbol{v}_{cmd}$ to the virtual control inputs $\boldsymbol{v}$. This is the input-output relationship shown on the left side of Figure 3.

B. Control allocation effectiveness metrics

This section proposes several metrics to quantify the effectiveness of the control allocation. Each proposed metric is expressed as some measure of $W(\rho)$ that quantifies its deviation from the ideal value of I_{n_v}. While some metrics help quantify overall allocation effectiveness, others provide more granular information on the direct control authority at a virtual control channel or severity of undesirable coupling among different channels.

1. Scale factor errors

The scale factor errors (SFE) are defined as the diagonal elements of $W(\rho)$. The minimum and maximum SFEs are:

$$\min \text{SFE} = \min \text{diag}(W(\rho)) \tag{3a}$$

$$\max \text{SFE} = \max \text{diag}(W(\rho)) \tag{3b}$$

where $\text{diag}(\cdot)$ extracts the diagonal elements of a square matrix. The minimum and maximum SFEs are important as they indicate the worst-case degradation in the direct control authority across all virtual control channels. Deviation of the SFEs from unity results in amplification or attenuation of the loop gain at the corresponding virtual control channel.

2. Off-diagonal norm

The off-diagonal norm γ is defined as the Frobenius norm of the off-diagonal elements of $W(\rho)$:

$$\gamma = \left\| W(\rho) - W(\rho) \circ I_{n_v} \right\|_F \tag{4}$$

where $\circ$ denotes the Hadamard product of two matrices. While the SFEs are useful in detecting degradation in the direct control authority of the virtual control channels, the off-diagonal norm metric detects undesirable coupling across channels. A perfect control allocation should yield $\gamma = 0$.

3. Singular values and condition number

The singular values of $W(\rho)$ offer insight on the directionality of the control allocation. They blend the impact of both the diagonal and the off-diagonal elements of $W(\rho)$. A related metric is the condition number, which is defined as the ratio between the maximum and minimum singular values:

$$\kappa = \frac{\overline{\sigma}\left(W(\rho)\right)}{\underline{\sigma}\left(W(\rho)\right)} \tag{5}$$

A large condition number ($\kappa \gg 1$) indicates strong directionality in the control allocation [19]. If this is caused by a large $\overline{\sigma}\left(W(\rho)\right)$, then an undesirable loop gain amplification is expected at one of the virtual control channels. On the other hand, if this is caused by a small $\underline{\sigma}\left(W(\rho)\right)$, then an undesirable loop gain attenuation is expected at one of the virtual control channels. Both of these scenarios deteriorate the overall effectiveness of control allocation.

4. Distance-to-identity

The distance-to-identity metric δ_I provides a direct measure of the deviation of $W(\rho)$ from I_{n_v}. It is defined as:

$$\delta_I = \left\| W(\rho) - I_{n_v} \right\|_F \tag{6}$$

C. Impact of actuator saturation and failures

Saturation or failure of one or more actuators may influence the control allocation effectiveness. Specifically, $\boldsymbol{h}_i = 0$ if the i^{th} actuator is saturated or failed.

1. Saturation or undetected failure

When there are undetected failures or saturation in one or more actuators, then there are two possibilities. If $n_u - n_{u_f} \geq n_v$, then the system will remain over-actuated or become fully-actuated. In this case, although $W(\rho)$ will remain full-rank, the control allocation effectiveness will deteriorate because $W(\rho)$ will deviate from I_{n_v}. On the other hand, if $n_u - n_{u_f} < n_v$, then the system will become under-actuated. In this case, $W(\rho)$ will become rank-deficient and the control allocation effectiveness will deteriorate significantly. The metrics developed in Section III can be used to assess the severity of the deterioration.

2. Detected failure

If the actuator failures are detected, then the control allocator can be redesigned accordingly. In the fully-actuated or over-actuated case ($n_u - n_{u_f} \geq n_v$), the updated $C(\rho_m)$ should prevent any degradation in the control allocation effectiveness. In the under-actuated case ($n_u - n_{u_f} < n_v$), the updated $C(\rho_m)$ would have to unallocate $n_v - (n_u - n_{u_f})$ control degrees of freedom based on their predetermined priority, yielding $\operatorname{rank} W(\rho) = n_u - n_{u_f}$. Although a rank-deficient $W(\rho)$ would result in degraded metrics, this would be misleading when the failures are detected, as the control reallocation would intentionally exclude some control degrees of freedom. This necessitates an adjustment to the computation of proposed metrics.

The unallocated control degrees of freedom could be selected arbitrarily in the basis that span the subspace $\mathbb{R}^{n_v}$, set by the virtual control commands. For simplicity, the scope of this paper is limited to the case where the unallocated control degrees or freedom are aligned with any of the virtual control commands. In this scenario, the adjustment is performed by computing the metrics from the sub-matrix $W'(\rho) \in \mathbb{R}^{(n_u - n_{u_f}) \times (n_u - n_{u_f})}$ of $W(\rho) \in \mathbb{R}^{n_v \times n_v}$, which is extracted by omitting the rows and the columns corresponding to the unallocated $n_v - (n_u - n_{u_f})$ control degrees of freedom. For demonstration purposes, let there be one virtual control command that is unallocated such that $n_v - (n_u - n_{u_f}) = 1$. Let l denote the index of the excluded virtual control command with $1 \leq l \leq n_v$. Then $W'(\rho) \in \mathbb{R}^{(n_v-1)\times(n_v-1)}$ is obtained after discarding l^{th} row and l^{th} column of $W(\rho)$.

$$W(\rho) = \left[\begin{array}{cccccc} w_{1,1} & w_{1,2} & \cdots & w_{1,l} & \cdots & w_{1,n_v} \\ w_{2,1} & w_{2,2} & \cdots & w_{2,l} & \cdots & w_{2,n_v} \\ \vdots & \vdots & \ddots & \vdots & \ddots & \vdots \\ \hline w_{l,1} & w_{l,2} & \cdots & w_{l,l} & \cdots & w_{l,n_v} \\ \hline \vdots & \vdots & \ddots & \vdots & \ddots & \vdots \\ w_{n_v,1} & w_{n_v,2} & \cdots & w_{n_v,l} & \cdots & w_{n_v,n_v} \end{array}\right] \tag{7}$$

3. Frequency-dependent metrics

The metrics described thus far are independent of frequency because the control allocator is assumed to be stateless (Assumption 3). If the control allocator includes dynamics, $C(s, \rho_m)$, then this will yield a frequency dependent commanded-to-actual virtual control matrix: $W(s, \rho) \coloneqq J(\rho) \cdot \operatorname{diag}(\boldsymbol{h}) \cdot C(s, \rho_m)$. In such a scenario, the metrics quantifying control allocation effectiveness would also vary with frequency. A detailed discussion on this topic is not within the scope of this paper and is deferred to a future study.

IV. Numerical example

The problem formulation described in Section II and the metrics described in Section III are illustrated using a lateral-directional flight dynamic model of a small fixed-wing unmanned aircraft called the UltraStick 25e that was reported in [18]. While the model reported in [18] used a single aileron and rudder, an additional aileron and rudder is added in this numerical example to make the system over-actuated. Each component of the closed-loop system shown in Figure 2 is described in the following subsections using the notation introduced in Section II.

A. Plant and actuator dynamics models

1. Plant model $G(s, \rho)$

The plant model $G(s, \rho)$ has the form:

$$M\dot{\boldsymbol{x}} = A'\boldsymbol{x} + B'\boldsymbol{u} \tag{8a}$$

$$\boldsymbol{y} = C\boldsymbol{x} \tag{8b}$$

where $\boldsymbol{x} = [v,\ p,\ r,\ \phi,\ \psi]^T \in \mathbb{R}^5$ is the state vector, $\boldsymbol{u} = \left[\delta_{a_1},\ \delta_{a_2},\ \delta_{r_1},\ \delta_{r_2}\right] \in \mathbb{R}^4$ is the true actuator input vector, and $\boldsymbol{y} = [p,\ r,\ \phi] \in \mathbb{R}^3$ is the output vector. The components of $\boldsymbol{x}$ include the lateral velocity v, roll rate p, yaw rate r, roll angle ϕ, and yaw angle ψ. The true actuator inputs include two different ailerons $\delta_{a_{1,2}}$ and two different rudders $\delta_{r_{1,2}}$.

The state-space matrices are given by:

$$M = \begin{bmatrix} 1 & 0 & 0 & 0 & 0 \\ 0 & 1 & -I_{xz}/I_x & 0 & 0 \\ 0 & -I_{xz}/I_z & 1 & 0 & 0 \\ 0 & 0 & 0 & 1 & 0 \\ 0 & 0 & 0 & 0 & 0 \end{bmatrix} \quad A' = \begin{bmatrix} Y_v & Y_p + w_0 & Y_r - u_0 & g\cos\theta_0 & 0 \\ L_v & L_p & L_r & 0 & 0 \\ N_v & N_p & N_r & 0 & 0 \\ 0 & 1 & 0.03 & 0 & 0 \\ 0 & 0 & 1 & 0 & 0 \end{bmatrix} \quad B' = \begin{bmatrix} Y_{\delta a_1} & Y_{\delta a_2} & Y_{\delta r_1} & Y_{\delta r_2} \\ L_{\delta a_1} & L_{\delta a_2} & L_{\delta r_1} & L_{\delta r_2} \\ N_{\delta a_1} & N_{\delta a_2} & N_{\delta r_1} & N_{\delta r_2} \\ 0 & 0 & 0 & 0 \\ 0 & 0 & 0 & 0 \end{bmatrix} \tag{9}$$

where I_x, I_z, and I_{xz} denote the components of the moment of inertia tensor, u_0, w_0, and θ_0 denote the trim parameters, and $Y_\star$, $L_\star$, and $N_\star$ denote the aerodynamic stability and control derivatives. The Appendix lists the values of all these parameters. The C matrix is not provided because it can be inferred from the $\boldsymbol{x}$ and $\boldsymbol{y}$ stated above. The feedthrough matrix D is zero.

2. Decomposition of $G(s, \rho)$

The plant model $G(s, \rho)$ is decomposed as the product $\bar{G}(s) \cdot J(\rho)$, where the virtual plant $\bar{G}(s)$ and the control Jacobian $J(\rho)$ have the state-space realizations:

$$M\dot{\boldsymbol{x}} = A'\boldsymbol{x} + B''\boldsymbol{v} \tag{10a}$$

$$\boldsymbol{v} = J(\rho)\boldsymbol{u} \tag{10b}$$

The three control degrees of freedom are spanned by the vector of virtual control inputs $\boldsymbol{v} = [\dot{v}_{cmd}, \dot{p}_{cmd}, \dot{r}_{cmd}] \in \mathbb{R}^3$ and the matrices B'' and $J(\rho)$ are given by:

$$B'' = \begin{bmatrix} 1 & 0 & 0 & 0 & 0 \\ 0 & 1 & 0 & 0 & 0 \\ 0 & 0 & 1 & 0 & 0 \end{bmatrix}^T \quad J(\rho) = \begin{bmatrix} Y_{\delta a_1} & Y_{\delta a_2} & Y_{\delta r_1} & Y_{\delta r_2} \\ L_{\delta a_1} & L_{\delta a_2} & L_{\delta r_1} & L_{\delta r_2} \\ N_{\delta a_1} & N_{\delta a_2} & N_{\delta r_1} & N_{\delta r_2} \end{bmatrix} \tag{11}$$

While each control derivative in $J(\rho)$ is a function of ρ, this functional dependence is suppressed in Equation (11) for brevity. The state-space realization of $\bar{G}(s)$ presented in Equation (1) is recovered by noting that $A = M^{-1}A'$ and $B = M^{-1}B''$.

3. Variation of $J(\rho)$ over the operating envelope $\mathcal{P}$

While the operating condition can be multi-dimensional in general, this numerical example considers a scalar operating condition $\rho \in \mathcal{P} \subseteq \mathbb{R}$ for simplicity. The operating envelope $\mathcal{P}$ is normalized to the interval $[-1, 1]$. The control Jacobian $J(\rho)$ is modeled to vary over $\mathcal{P} = [-1, 1]$ using the aerodynamic parameter uncertainties reported in [18]. Specifically, each control derivative in $J(\rho)$ is assumed to vary linearly in the interval $[\mu - 6\sigma, \mu + 6\sigma]$ as ρ varies in the interval $\mathcal{P} = [-1, 1]$. The Appendix lists the values of the mean μ and the standard deviation σ for each control derivative.

4. Actuator dynamics model $\Lambda(s)$

The actuator dynamics $\Lambda(s)$ is modeled as: $\Lambda(s) = \bar{\Lambda}(s) \cdot I_4$, where

$$\bar{\Lambda}(s) = e^{-0.05s}\frac{2\pi 10}{s + 2\pi 10} \tag{12}$$

is the single-channel actuator dynamic model with a bandwidth of 10 Hz and a time delay of 50 ms.

B. Feedback controller $\bar{K}(s)$

The feedback controller $\bar{K}(s)$ is designed using the virtual plant $\bar{G}(s)$, as shown on the right side of Figure 3. $\bar{K}(s)$ has the following form:

$$\begin{bmatrix} \dot{v}_{cmd} \\ \dot{p}_{cmd} \\ \dot{r}_{cmd} \end{bmatrix} = \begin{bmatrix} 0 & K_{\dot{v}\phi} & 0 & 0 \\ K_{\dot{p}\phi}(s) & -K_{\dot{p}\phi}(s) & K_{\dot{p}p} & 0 \\ 0 & 0 & 0 & K_{\dot{r}r} \end{bmatrix} \begin{bmatrix} \phi_{cmd} \\ \phi \\ p \\ r \end{bmatrix} \tag{13}$$

where its inputs consist of $\boldsymbol{r} = \phi_{cmd}$ and $\boldsymbol{y} = [p,\ r,\ \phi]$ and its outputs consist of the virtual control commands $\boldsymbol{\nu}_{cmd} = [\dot{v}_{cmd},\ \dot{p}_{cmd},\ \dot{r}_{cmd}]$. The term $K_{\dot{p}\phi}(s)$ in Equation (13) denotes a PI controller whereas all the other terms denote static gains.

The gains of $\bar{K}(s)$ are tuned using the virtual plant $\bar{G}(s)$ to satisfy the following user-defined closed-loop performance and robustness requirements.

1) Bandwidth of at least 6 rad s^{-1} in the $\dot{p}_{cmd}$ control degree of freedom, as measured using the gain crossover frequency of the corresponding open-loop transfer function.
2) Rise time of at most 1 s in ϕ when tracking a step command in ϕ_{cmd}.
3) No overshoot in ϕ when tracking a step command in ϕ_{cmd}.
4) Gain margin of at least 6 dB, phase margin of at least 45 deg, and disk margin [21] of at least 0.5, as measured using the open-loop transfer functions obtained by breaking the loop at each of the three virtual control commands $\boldsymbol{\nu}_{cmd} = [\dot{v}_{cmd},\ \dot{p}_{cmd},\ \dot{r}_{cmd}]$.
5) Damping ratio of at least 0.7 for every closed-loop pole.

The gains of $\bar{K}(s)$ are tuned using basic loopshaping techniques [22, 23] and are provided in the Appendix.

C. Control allocator $C(\rho_m)$

The control allocator $C(\rho_m)$ is designed using the control Jacobian $J(\rho)$, as shown on the left side of Figure 3. While the literature provides many techniques to design control allocators, a simple technique based on the pseudo-inverse of $J(\rho)$ is considered in this numerical example. In this regard, the metrics proposed in Section III are not restricted to any particular design technique and may be computed as long as the control allocator can be linearized. For the purpose of this numerical example, three separate control allocators are designed, as explained next.

1. Nominal control allocator

The nominal control allocator C_{nom} does not have access to a measurement of the operating condition ρ_m. It is designed using the right-inverse of the control Jacobian J_0 obtained at the nominal operating condition $\rho = 0$.

$$C_{nom} = J_0^{\dagger} = J_0^T\,(J_0 J_0^T)^{-1} \tag{14}$$

2. Scheduled control allocator

The scheduled control allocator $C(\rho_m)$ uses the imperfect measurement

$$\rho_m = \max\,(-1,\ \min\,(1,\ \sinh\rho)) \tag{15}$$

of the operating condition ρ, where the ρ_m is clipped to lie within the operating envelope $\mathcal{P} = [-1,\ 1]$. Figure 4 shows the relationship between ρ, $\sinh\rho$, and ρ_m. The control allocator is designed by gridding the operating envelope $\mathcal{P}$ into a discrete set of N operating conditions $\{\rho_i \in \mathcal{P}\}_{i=1}^{N}$ and computing $C_i = J(\rho_i)^{\dagger}$ at each grid point ρ_i. At any intermediate measured operating condition $\rho_i \le \rho_m \le \rho_{i+1}$, $C(\rho_m)$ is obtained by linearly interpolating between the control allocators C_i and C_{i+1} computed at the neighboring grid points. In this example, $\mathcal{P}$ is gridded into the three grid points $\{-1,\ 0,\ 1\}$. An alternative scheduling strategy is to linearly interpolate between the control Jacobians $J(\rho_i)$ and $J(\rho_{i+1})$ at the neighboring grid points and compute the control allocator as its right-inverse. The approach taken in this paper of directly interpolating between the control allocators is simply a design choice.

3. Degraded control allocator

The degraded control allocator $\bar{C}(\rho_m)$ is used when there are *detected* failures in one or more actuators, as indicated by the presence of zeros in the vector $\boldsymbol{h}$. This leads to two possibilities. If there are at least as many healthy actuators as there are control degrees of freedom ($n_u - n_{u_f} \ge n_\nu$), then the system remains over-actuated or fully-actuated, in which case all the control degrees of freedom may be allocated among the healthy actuators. On the other hand, if there are fewer healthy actuators than there are control degrees of freedom ($n_u - n_{u_f} < n_\nu$), then the system becomes under-actuated, in which case $n_\nu - (n_u - n_{u_f})$ control degrees of freedom need to be excluded from the allocation. To generalize this, let $\boldsymbol{d} \in \mathbb{R}^{n_\nu}$ denote a vector of ones and zeros, where ones include and zeros exclude control degrees of freedom from the allocation. The degraded control allocator at the grid point ρ_i is designed as:

$$\bar{C}_i = (\mathrm{diag}(\boldsymbol{d}) \cdot J(\rho_i) \cdot \mathrm{diag}(\boldsymbol{h}))^{\dagger} \tag{16}$$

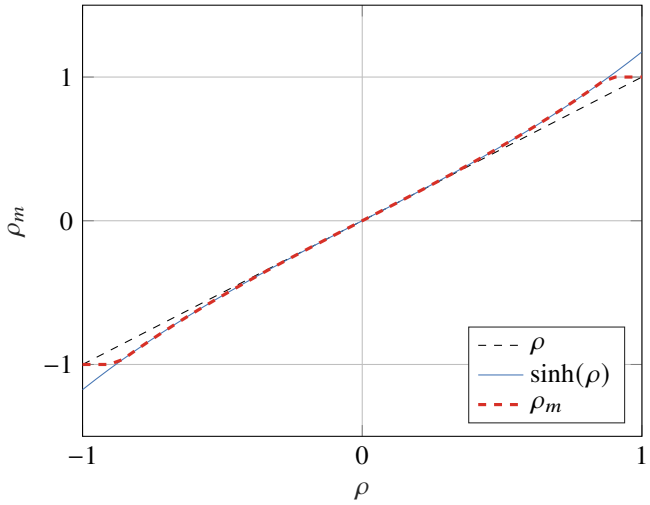

Fig. 4 Relationship between true and imperfect measurements.

At any intermediate measured operating condition $\rho_i \leq \rho_m \leq \rho_{i+1}$, $\bar{C}(\rho_m)$ is obtained by linearly interpolating between the degraded control allocators $\bar{C}_i$ and $\bar{C}_{i+1}$ computed at the neighboring grid points. As with the scheduled control allocator, the approach taken in this paper of directly interpolating between the control allocators, as opposed to the control Jacobians, is simply a design choice.

V. Results

In this section, the numerical example introduced in Section IV is used to illustrate the contributions of this paper. First, the relationship between proposed allocation effectiveness metrics and linear closed-loop stability and performance metrics is discussed in Section V.A, followed by the effect of control allocator scheduling on these metrics in Section V.B. The influence of control derivative reversals on the proposed allocation effectiveness metrics is investigated in Section V.C. In Section V.D, impact of an undetected actuator failure yielding a fully actuated system on the control allocation metrics is studied. Finally, the adjustment required to compute the proposed metrics in the event of detected actuator failures leading to an under-actuated system is discussed in Section V.E.

A. Correlation between proposed metrics and linear closed-loop metrics

The variation in control derivatives across the normalized operating envelope $\mathcal{P} = [-1,\ 1]$ is provided in Figure 5. Blue and red colors represent the intervals $\mathcal{P}_- = [-1,\ 0]$ and $\mathcal{P}_+ = [0,\ 1]$. The nominal control allocator, C_{nom}, is designed at $\rho = 0$ (i.e., $\mathcal{P}_0$) and does not take into account the control derivative variations across $\mathcal{P}$. This deteriorates the allocation effectiveness, which is captured by divergence of the metrics proposed in Section III: min SFE, max SFE, κ, γ, δ_I, from their ideal values (see Table 1 for design values of each metric). This is depicted in Figure 6, where the proposed metrics for C_{nom} are plotted against $L_{\delta a}$ with solid lines.

Next, the relationship between proposed metrics that quantify the control allocation effectiveness and key closed-loop stability and performance metrics are investigated. Specifically, the disk margin [21] and the gain crossover frequency ω_{pm+} associated with the positive phase margin (indicating the bandwidth) at the $\dot{p}_{cmd}$, ϕ, and $\dot{r}_{cmd}$ loop cuts are selected as the closed-loop metrics of interest. Figure 7 displays the variation in the disk margin at $\dot{p}_{cmd}$, ϕ, and $\dot{r}_{cmd}$ loop cuts with respect to the proposed metrics. Similarly, in Figure 8, the gain crossover frequency associated with the positive phase margin at $\dot{p}_{cmd}$, ϕ, and $\dot{r}_{cmd}$ loop cuts are plotted against these metrics. In both figures, the results for C_{nom} are represented with solid lines.

As the operating condition departs from $\mathcal{P}_0$ and min SFE, max SFE, κ, γ, δ_I diverge from their ideal values, control allocation effectiveness degrades. In the meanwhile, it is also evident that the closed-loop metrics deviate from their

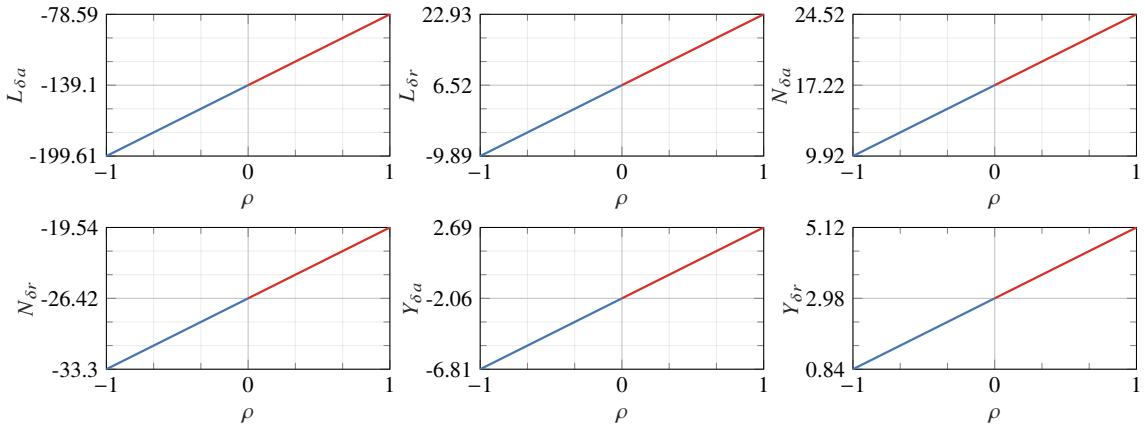

Fig. 5 Variation of control derivatives across the normalized operating envelope $\mathcal{P}$. Blue (——) and red (——) colors represent intervals $\mathcal{P}_-$ and $\mathcal{P}_+$.

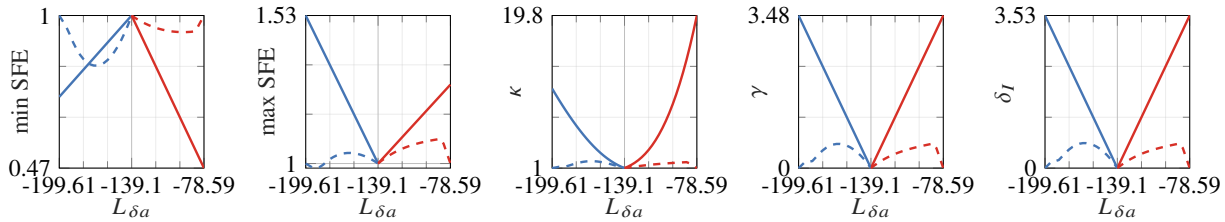

Fig. 6 Proposed metrics indicating control allocation effectiveness vs. $L_{\delta a}$ (variations in other control derivatives can be found in Figure 5). Solid and dashed lines depict the results with nominal and scheduled control allocators, respectively. Blue (——) and red (——) colors represent normalized operating envelope intervals $\mathcal{P}_-$ and $\mathcal{P}_+$.

nominal design values. In particular, deterioration takes place in disk margin across $\mathcal{P}_-$ and ω_{pm+} across $\mathcal{P}_+$ at $\dot{p}_{cmd}$, ϕ, and $\dot{r}_{cmd}$ loop cuts. Worst-case control allocation effectiveness and closed-loop metrics with C_{nom} across the operating envelope are provided at Table 1 along with their design (ideal) values.

Table 1 Worst-case metrics across the operating envelope with nominal and scheduled control allocators.

Metric	Design Value at $\mathcal{P}_0$	Worst-case Value with C_{nom}	Worst-case Value with $C(\rho_m)$
min SFE	1	-0.47 ($\rho = 1$)	0.83 ($\rho = -0.48$)
max SFE	1	1.53 ($\rho = -1$)	1.09 ($\rho = 0.86$)
κ	1	19.8 ($\rho = 1$)	1.85 ($\rho = -0.48$)
γ	0	3.48 ($\rho = -1$)	0.56 ($\rho = 0.86$)
δ_I	0	3.53 ($\rho = -1$)	0.58 ($\rho = -0.48$)
Disk M. at $\dot{p}_{cmd}$	0.61	0.39 ($\rho = -1$)	0.58 ($\rho = 0.86$)
ω_{pm+} at $\dot{p}_{cmd}$ (rad/s)	6.49	1.49 ($\rho = 1$)	6.02 ($\rho = -0.86$)

B. Effectiveness of scheduled control allocator

Next, influence of scheduled control allocator, $C(\rho_m)$, on the allocation effectiveness and closed-loop metrics is analyzed. The results with $C(\rho_m)$ are represented in Figures 6, 7, and 8 with dashed lines. Figure 6 shows that deviation

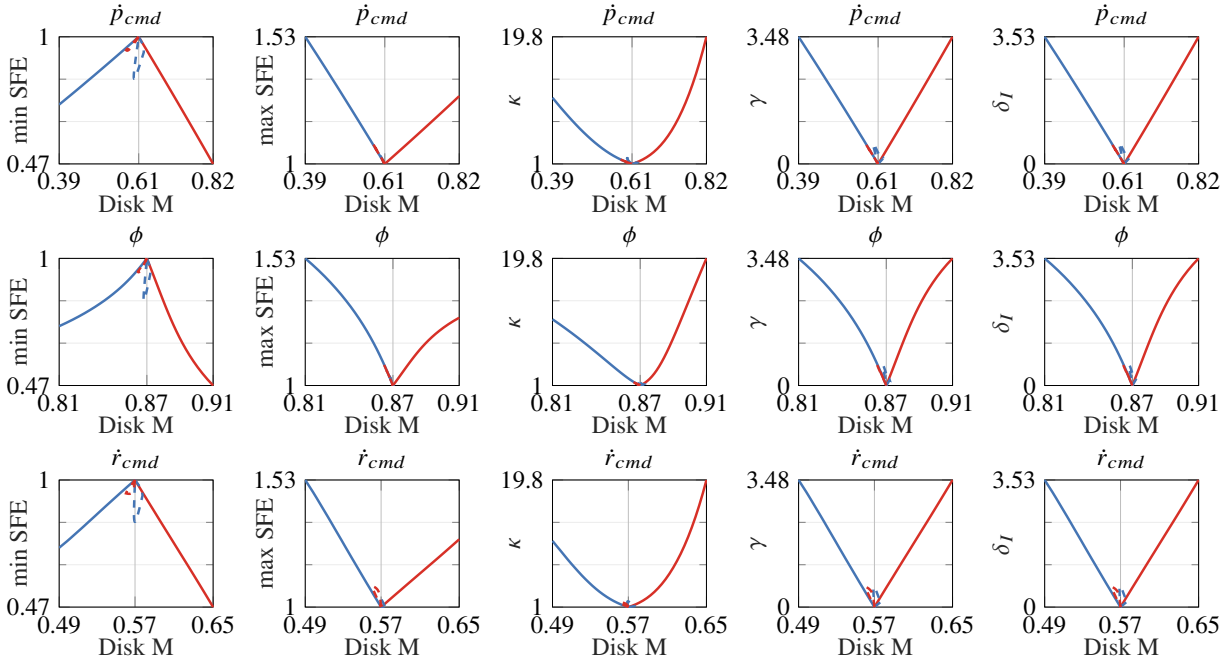

Fig. 7 Proposed metrics indicating control allocation effectiveness vs. disk margin at $\dot{p}_{cmd}$, ϕ, and $\dot{r}_{cmd}$ loop cuts. Blue (—) and red (—) colors represent normalized operating envelope intervals $\mathcal{P}_-$ and $\mathcal{P}_+$. Solid and dashed lines depict results with nominal and scheduled control allocator.

of the proposed metrics, min SFE, max SFE, κ, γ, δ_I, from their ideal values across $\mathcal{P}$ is quite limited with $C(\rho_m)$ compared to C_{nom}. This suggests notable improvement in the control allocation effectiveness. Similar observation can be made for the closed-loop metrics according to Figures 7 and 8. Departure of the disk margin and ω_{pm+} from their design values substantially diminishes upon scheduling of the control allocator. In Table 1, the worst-case metrics with C_{nom} and $C(\rho_m)$ across $\mathcal{P}$ are tabulated, which quantify these observations.

C. Detection of reversals in the control effectiveness of actuators

Aileron control effectiveness sign reversal is a phenomenon observed in fixed-wing aircraft with high-aspect ratio, flexible wings [24]. This section assesses the impact of aileron control effectiveness sign reversal on the overall control allocation effectiveness by varying $L_{\delta a}$. Different from the numerical examples used in Sections V.A and V.B, here, only $L_{\delta a}$ is swept from its nominal value at $\mathcal{P}_0$ towards 0, while the remaining control derivatives are unchanged.

Figure 9 shows divergence of the proposed metrics, min SFE, κ, γ, δ_I, from their nominal values as $L_{\delta a}$ is swept towards 0. In particular, min SFE metric approaches 0 as $L_{\delta a}$ approaches 0, indicating notable attenuation in loop gain at a virtual control channel. Examination of the commanded-to-actual virtual control matrix suggests that decreasing min SFE corresponds to the $\dot{p}_{cmd}$ channel. In addition, κ increases rapidly, pointing to strengthening directionality in control allocation. Furthermore, increase in γ suggests that as direct control authority degrades at $\dot{p}_{cmd}$ virtual control channel, undesirable coupling across different channels emerges. The degrading control allocation effectiveness presents itself in the ω_{pm+} at $\dot{p}_{cmd}$, ϕ, and $\dot{r}_{cmd}$ loop cuts, as depicted in Figure 10. The bandwidth at $\dot{p}_{cmd}$, ϕ loop cuts approach to 0 as does min SFE. Accordingly, as shown in Figure 11, the steady-state error in step response of ϕ with respect to ϕ_{cmd} increases as $L_{\delta a}$ approaches 0 and, as its sign reverses, the system becomes unstable.

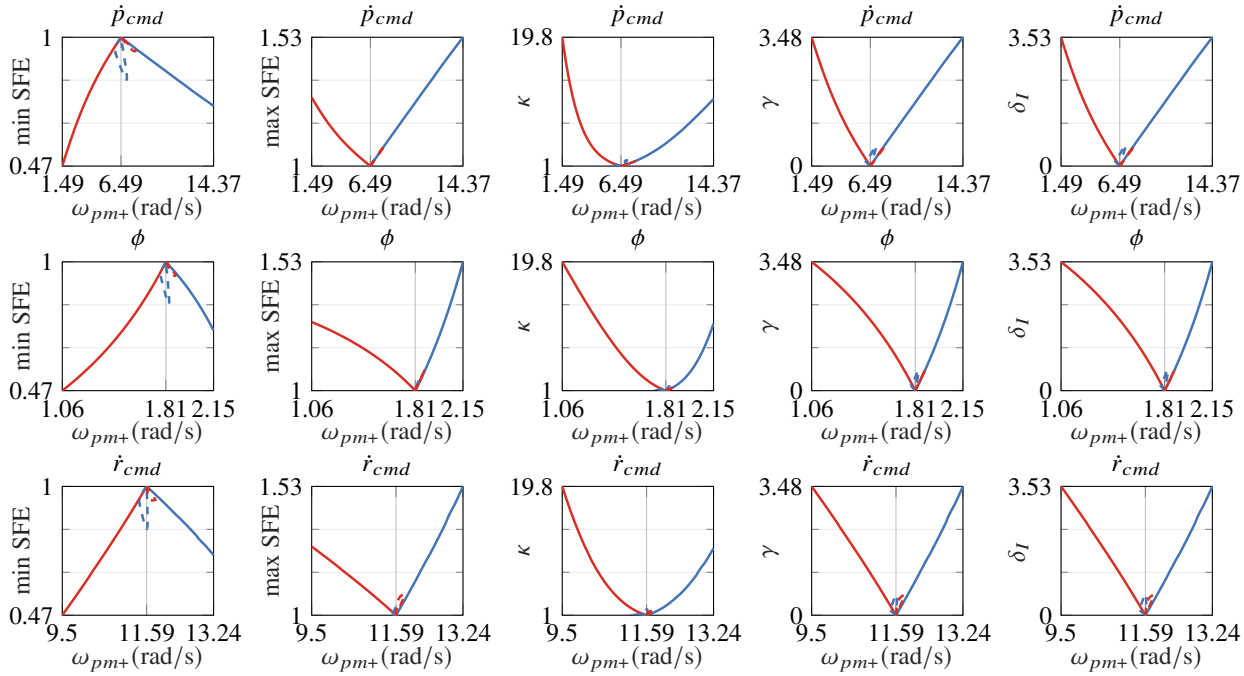

Fig. 8 Proposed metrics indicating control allocation effectiveness vs. gain crossover frequency associated with the positive phase margin at $\dot{p}_{cmd}$, ϕ, and $\dot{r}_{cmd}$ loop cuts. Blue (——) and red (——) colors represent normalized operating envelope intervals $\mathcal{P}_-$ and $\mathcal{P}_+$. Solid and dashed lines depict results with nominal and scheduled control allocator.

D. Impact of undetected actuator failure on control allocation effectiveness

Next, an analysis is performed to assess how the proposed metrics degrade when the control allocator is unaware of actuator failures. For this scenario, one of the rudders, δ_{r_1}, is considered to be failed, yielding a fully actuated system with $n_u = n_v = 3$. A scheduled control allocator, $C(\rho_m)$, is used across the operating envelope, $\mathcal{P}$. To study the effect of undetected actuator failure on control allocation effectiveness, the proposed metrics are compared between two cases: (i) undetected actuator failure and (ii) detected actuator failure with a control reallocation as described in Section IV.C.3.

Figure 12 depicts how min SFE, max SFE, κ, γ and δ_I vary across $\mathcal{P}$ with undetected (solid lines) and detected (dashed lines) δ_{r_1} failures. While all proposed metrics diverge from their ideal values for the undetected case, it is worth noting that min SFE decreases to -0.44 in $\mathcal{P}_+$. The sign reversal suggests that the used control allocator is a poor candidate with δ_{r_1} failure. The influence of degraded allocation effectiveness is evident in the disk margin deterioration to 0.2 at $\dot{r}_{cmd}$ loop cut. In contrast, upon detection of the failure and corresponding control reallocation, both proposed metrics and the disk margin at $\dot{r}_{cmd}$ loop cut show improvement with limited variance from their design values.

E. Adjustment of metrics to account for detected actuator failures leading to under-actuation

In this section, the adjustment required on the computation of proposed metrics is discussed in the event of detected actuator failures leading to under-actuation. For this scenario, one rudder δ_{r_2} and one aileron δ_{a_2} are considered to be failed, yielding an under-actuated system with $n_u = 2$ and $n_v = 3$. To address the under-actuation, a control reallocation is performed that excludes the $\dot{v}_{cmd}$ control degree of freedom. Furthermore, it is considered that this control allocator does not have access to a measurement of the operating condition.

As discussed in Section III.C.2, the proposed metrics need to be computed from submatrix $W'(\rho) \in \mathbb{R}^{2\times2}$ of $W(\rho) \in \mathbb{R}^{3\times3}$, which is extracted by omitting the rows and the columns corresponding to the removed control degree of freedom. This operation is presented in Equation (17) at the design condition $\mathcal{P}_0$, and its impact on the allocation

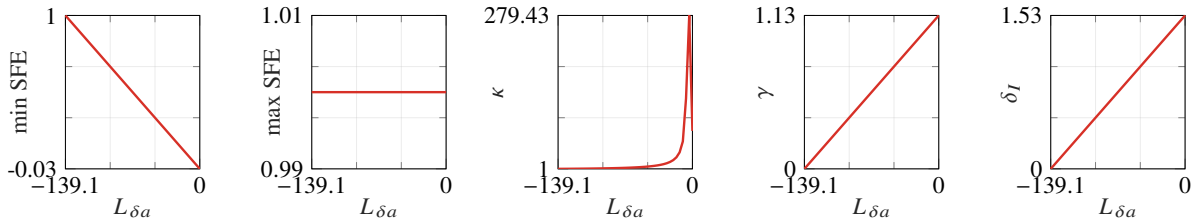

Fig. 9 Proposed metrics indicating control allocation effectiveness vs. $L_{\delta a}$, as $L_{\delta a}$ is swept from its nominal value at $\mathcal{P}_0$ towards 0.

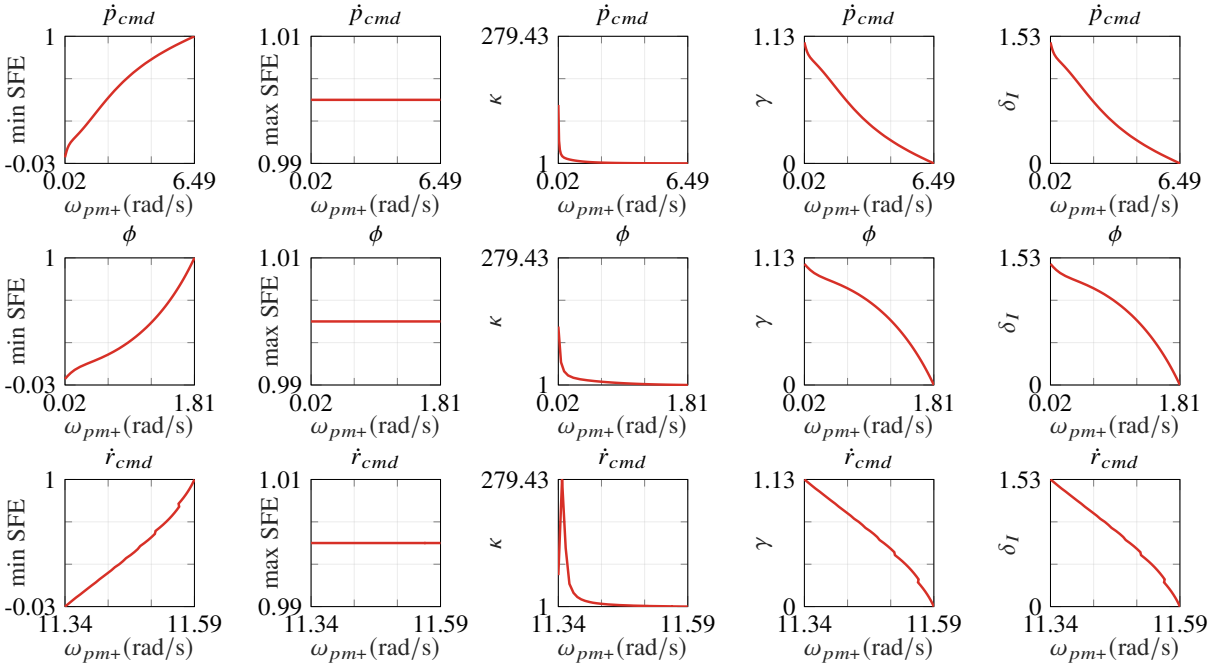

Fig. 10 Proposed metrics indicating control allocation effectiveness vs. gain crossover frequency associated with the positive phase margin at $\dot{p}_{cmd}$, ϕ, and $\dot{r}_{cmd}$ loop cuts. Results are obtained by sweeping $L_{\delta a}$ from its nominal value at $\mathcal{P}_0$ towards 0, while other control derivatives are unchanged.

effectiveness metrics is depicted in Figure 13.

$$W(0) = \begin{bmatrix} 0 & 0.001 & -0.1689 \\ 0 & 1 & 0 \\ 0 & 0 & 1 \end{bmatrix} \tag{17}$$

In Figure 13, variation of min SFE, max SFE, κ, γ and δ_I metrics across $\mathcal{P}$ is plotted without (solid lines) and with (dashed lines) the adjustment. At $\mathcal{P}_0$, adjusted metrics are at their design values as expected, while the unadjusted metrics are off. Note that min SFE = 0 given the first diagonal element of $W(0)$ in Equation (17) when the adjustment is ignored. Furthermore, while not visualized on the figure, $\kappa \to \infty$ due to the rank deficient $W(0)$. These issues are resolved when the metrics are computed from the submatrix $W'(0) = I_2$.

Disk margin at $\dot{p}_{cmd}$ loop cut is identical in both cases across $\mathcal{P}$. This is expected, as only difference between two cases is in the computation of control allocation metrics which affects neither the control allocator nor the rest of

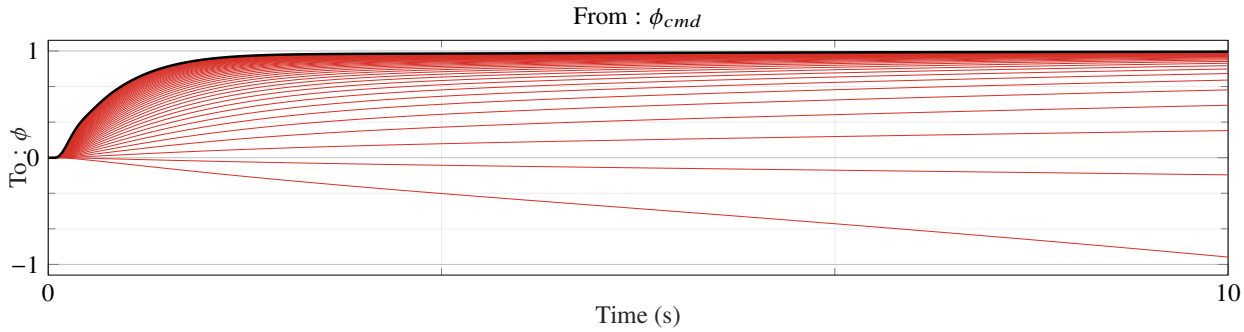

Fig. 11 Step response of ϕ with respect to ϕ_{cmd}. Black colored line represents the response at $\mathcal{P}_0$, while red colored lines represent the response as $L_{\delta a}$ is swept towards 0.

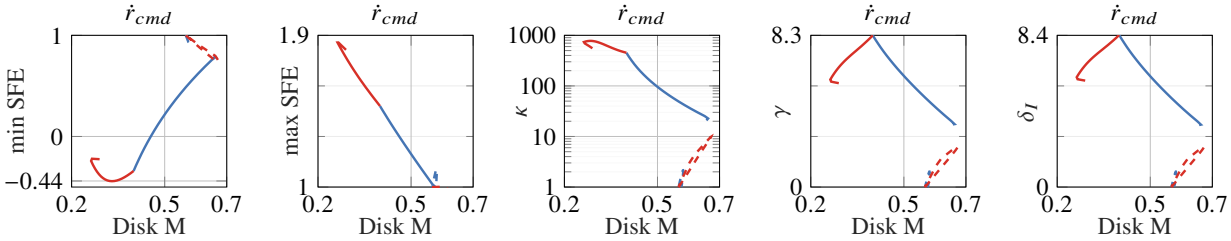

Fig. 12 Proposed metrics indicating control allocation effectiveness vs. disk margin at $\dot{r}_{cmd}$ loop cut. Blue (——) and red (——) colors represent normalized operating envelope intervals $\mathcal{P}_-$ and $\mathcal{P}_+$. Solid and dashed lines depict undetected and detected δ_{r_1} failure.

closed-loop system. In addition, max SFE with and without the adjustment are identical across $\mathcal{P}$, as max SFE is not affected by the omitted row or column.

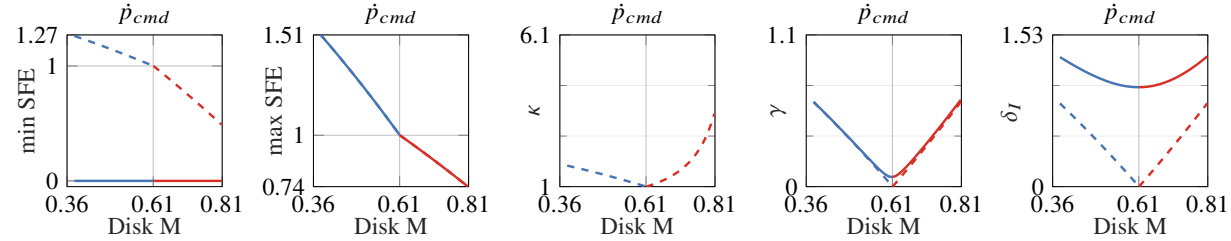

Fig. 13 Proposed metrics indicating control allocation effectiveness vs. disk margin at $\dot{p}_{cmd}$ loop cut. Blue (——) and red (——) colors represent normalized operating envelope intervals $\mathcal{P}_-$ and $\mathcal{P}_+$. Solid and dashed lines depict unadjusted and adjusted allocation effectiveness metrics. δ_{α_2} and δ_{r_2} have failed in this case and the control allocator, without access to ρ_m, is designed to unallocate $\dot{v}_{cmd}$ control degree of freedom.

VI. Conclusions

This paper proposes various metrics that measure the effectiveness of control allocation. These metrics are computed from the respective linearizations of the plant and the control allocation algorithm. They are shown to be correlated with the linear closed-loop performance and robustness metrics, as well as the grid density of the variables used to schedule the control allocation algorithm. In addition, the proposed metrics can be used to detect sign reversals in the control

effectiveness of individual actuators. The paper shows that the metrics may be adjusted such that they remain useful as a measure of the effectiveness of control allocation even under actuator saturations or failures. The proposed metrics not only provide the means to assess the control allocation effectiveness and its impact on the closed-loop performance and robustness metrics, but they can also guide the design of control allocation algorithms.

Appendix

Table 2 lists the values of the inertial and trim parameters referenced previously in Equation (9).

Table 2 Inertial and trim parameters.

Parameter	Value
I_x	0.089 kg m^2
I_y	0.144 kg m^2
I_z	0.162 kg m^2
I_{xz}	0.014 kg m^2
g	9.81 m s^{-2}
u_0	18.4 m s^{-1}
w_0	4.74 m s^{-1}
θ_0	14.4 deg

Table 3 lists the values of the aerodynamic stability and control derivatives referenced previously in Equation 9.

Table 3 Aerodynamic stability and control derivatives.

Parameter	Nominal value (μ)	Percent standard deviation $\left(\frac{\sigma}{\mu} \times 100\right)$
Y_v	−0.64	5.17
L_v	−2.02	9.16
N_v	1.30	3.49
Y_p	−4.28	20.20
L_p	−12.47	8.20
N_p	0.86	16.30
Y_r	0.19	0.74
L_r	4.05	16.82
N_r	−3.09	6.58
Y_{δ_a}	−2.06	38.42
L_{δ_a}	−139.10	7.25
N_{δ_a}	17.2	7.07
Y_{δ_r}	2.98	11.96
L_{δ_r}	6.52	41.94
N_{δ_r}	−26.4	4.34

The control derivatives of the individual ailerons $\delta_{a_{1,2}}$ and rudders $\delta_{r_{1,2}}$ are related to the values in Table 3 as follows.

$$B' = \begin{bmatrix} Y_{\delta a_1} & Y_{\delta a_2} & Y_{\delta r_1} & Y_{\delta r_2} \\ L_{\delta a_1} & L_{\delta a_2} & L_{\delta r_1} & L_{\delta r_2} \\ N_{\delta a_1} & N_{\delta a_2} & N_{\delta r_1} & N_{\delta r_2} \\ 0 & 0 & 0 & 0 \\ 0 & 0 & 0 & 0 \end{bmatrix} = \begin{bmatrix} 0.6\,Y_{\delta a} & 0.4\,Y_{\delta a} & 0.6\,Y_{\delta r} & 0.4\,Y_{\delta r} \\ 0.5\,L_{\delta a} & 0.5\,L_{\delta a} & 0.5\,L_{\delta r} & 0.5\,L_{\delta r} \\ 0.4\,N_{\delta a} & 0.6\,N_{\delta a} & 0.4\,N_{\delta r} & 0.6\,N_{\delta r} \\ 0 & 0 & 0 & 0 \\ 0 & 0 & 0 & 0 \end{bmatrix} \tag{18}$$

Table 4 lists the gains of the feedback controller $\bar{K}(s)$.

Table 4 Gains of the feedback controller $\bar{K}(s)$.

Gain	Value
$K_{\dot{\psi}\phi}$	−0.2
$K_{\dot{p}\phi}(s)$	$40 + \frac{8}{s}$
$K_{\dot{p}p}$	−12
$K_{\dot{r}r}$	−10

Acknowledgments

This work was funded by Amazon.com Services LLC.

References

[1] Yeh, Y. C., "Triple-triple redundant 777 primary flight computer," *1996 IEEE Aerospace Applications Conference. Proceedings*, Vol. 1, 1996, pp. 293–307 vol.1. https://doi.org/10.1109/AERO.1996.495891.

[2] Nguyen, N. T., Ting, E., Chaparro, D., Drew, M. C., and Shan-Min Swei, S., "Multi-Objective Flight Control for Drag Minimization and Load Alleviation of High-Aspect Ratio Flexible Wing Aircraft," *58th AIAA/ASCE/AHS/ASC Structures, Structural Dynamics, and Materials Conference*, 2007. https://doi.org/10.2514/6.2017-1589.

[3] Boskovic, J. D., and Mehra, R. K., "Control allocation in overactuated aircraft under position and rate limiting," *Proceedings of the 2002 American Control Conference (IEEE Cat. No.CH37301)*, Vol. 1, 2002, pp. 791–796 vol.1. https://doi.org/10.1109/ACC.2002.1024911.

[4] Blight, J. D., Dailey, R. L., and Gangsaas, D., "Practical control law design for aircraft using multivariable techniques," *International Journal of Control*, Vol. 59, No. 1, 1994, pp. 93–137. https://doi.org/10.1080/00207179408923071.

[5] Leith, D. J., and Leithead, W. E., "Survey of gain-scheduling analysis and design," *International Journal of Control*, Vol. 73, No. 11, 2000, pp. 1001–1025. https://doi.org/10.1080/002071700411304.

[6] Horn, R. A., and Johnson, C. R., *Matrix Analysis*, Cambridge University Press, 1985. https://doi.org/10.1017/CBO9780511810817.

[7] Adams, R. J., Buffington, J. M., Sparks, A. G., and Banda, S. S., *Robust Multivariable Flight Control*, Springer London, 1994. https://doi.org/10.1007/978-1-4471-2111-4.

[8] Durham, W. C., "Constrained control allocation," *Journal of Guidance, Control, and Dynamics*, Vol. 16, No. 4, 1993, pp. 717–725. https://doi.org/10.2514/3.21072.

[9] Bodson, M., "Evaluation of Optimization Methods for Control Allocation," *Journal of Guidance, Control, and Dynamics*, Vol. 25, No. 4, 2002, pp. 703–711. https://doi.org/10.2514/2.4937.

[10] Bodson, M., and Frost, S. A., "Load Balancing in Control Allocation," *Journal of Guidance, Control, and Dynamics*, Vol. 34, No. 2, 2011, pp. 380–387. https://doi.org/10.2514/1.51952.

[11] Poonamallee, V. L., Yurkovich, S., Serrani, A., and Doman, D. B., "A nonlinear programming approach for control allocation," *Proceedings of the 2004 American Control Conference*, Vol. 2, 2004, pp. 1689–1694 vol.2. https://doi.org/10.23919/ACC.2004.1386822.

[12] Johansen, T. A., Fossen, T. I., and Berge, S. P., "Constrained nonlinear control allocation with singularity avoidance using sequential quadratic programming," *IEEE Transactions on Control Systems Technology*, Vol. 12, No. 1, 2004, pp. 211–216. https://doi.org/10.1109/TCST.2003.821952.

[13] Yang, Y., and Gao, Z., "A New Method for Control Allocation of Aircraft Flight Control System," *IEEE Transactions on Automatic Control*, Vol. 65, No. 4, 2020, pp. 1413–1428. https://doi.org/10.1109/TAC.2019.2918122.

[14] Johansen, T. A., and Fossen, T. I., "Control allocation – A survey," *Automatica*, Vol. 49, No. 5, 2013, pp. 1087–1103. https://doi.org/https://doi.org/10.1016/j.automatica.2013.01.035.

[15] Zhang, Y., Sivasubramaniam, S. V., Jiang, B., and Theilliol, D., "Reconfigurable Control Allocation against Aircraft Control Effector Failures," *2007 IEEE International Conference on Control Applications*, 2007, pp. 1197–1202. https://doi.org/10.1109/CCA.2007.4389398.

[16] Ducard, G. J. J., *Fault-Tolerant Flight Control and Guidance Systems: Practical Methods for Small Unmanned Aerial Vehicles*, Springer, 2009.

[17] Tohidi, S. S., and Yildiz, Y., "Discrete Adaptive Control Allocation," *2021 American Control Conference (ACC)*, 2021, pp. 3731–3736. https://doi.org/10.23919/ACC50511.2021.9482628.

[18] Dorobantu, A., "Test Platforms for Model-Based Flight Research," Ph.D. thesis, University of Minnesota, Twin Cities, 2013.

[19] Skogestad, S., and Postlethwaite, I., *Multivariable Feedback Control: Analysis and Design*, Wiley, 2005.

[20] Durham, W., Bordignon, K. A., and Beck, R., *Aircraft Control Allocation*, Wiley, 2017.

[21] Seiler, P., Packard, A., and Gahinet, P., "An Introduction to Disk Margins [Lecture Notes]," *IEEE Control Systems Magazine*, Vol. 40, No. 5, 2020, pp. 78–95. https://doi.org/10.1109/MCS.2020.3005277.

[22] Åström, K. J., and Murray, R. M., *Feedback Systems*, Princeton University Press, 2019.

[23] Doyle, J., Francis, B., and Tannenbaum, A., *Feedback Control Theory*, Macmillan Publishing Company, 1990.

[24] Bueno, D. D., and Dowell, E. H., "Revisiting the Fundamentals of Control Surface Reversal Including Nonlinear Effects," *Journal of Aircraft*, Vol. 57, No. 6, 2020, pp. 1212–1219. https://doi.org/10.2514/1.C035885.